3D soft auxetic lattice structures fabricated by selective laser sintering: TPU powder evaluation and process optimization

Shangqin Yuan [a], Fei Shen [a], Jiaming Bai [b], Chee Kai Chua [a,*], Jun Wei [b], Kun Zhou [a,*]

[a] Singapore Centre for 3D Printing, School of Mechanical and Aerospace Engineering, Nanyang Technological University, Singapore 639798, Singapore
[b] Singapore Institute of Manufacturing Technology, Singapore 638075, Singapore

A B S T R A C T

The auxetic foams composed of highly porous thermoplastic polyurethane (TPU) exhibit an attractive behaviour of withstanding a large volume reduction upon the cyclic compressive loading. A family of three-dimensional (3D) artificial metamaterials via Bucklicrystals consisting of an array of elastomeric spherical shells with periodical lattice patterns were proposed to mimic the buckling-induced auxetic behaviour as TPU foams. Layer-by-layer deposition of the desirable materials to manufacture parts known as additive manufacturing enables to create complex geometries and provides the broad freedom in design and manufacturing. In this work, selective laser sintering offered a unique capability to fabricate tailorable and flexible 3D soft metamaterials using TPU powders. An effective method was proposed to systematically evaluate the TPU powders and optimize the fabrication process, in order to overcome the challenges of sintering the duel-segment TPU. The laser-sintered Bucklicrystals were highly recoverable undergoing repeated compressions, and they retained the auxetic properties over a wide range of applied deformations. The fabrication of 3D soft metamaterials is not constrained by existing manufacturing principles and the laser-sintered Bucklicrystals of TPU are highly valuable to various engineering applications, such as mechanical and acoustic energy absorbers, actuators and vibration-resistant dampers.

© 2017 Elsevier Ltd. All rights reserved.

1. Introduction

Additive manufacturing (AM) techniques, or three-dimensional (3D) printing techniques, offer great freedom of both design and manufacturing to fabricate products of complex geometries that have potential applications in device fabrication, tissue engineering, aerospace, automobile, etc. [1–7]. These techniques enable the concept of Manufacturing for Design to adapt into the future industries and daily life. In order to implement this new generation of design concept, a systematic integration of AM technique selection, material evaluation and structural modelling is of significance to the successfully production of desirable end-use functional products.

A 3D mechanical metamaterial contrasts in the transverse direction when subject to a uniaxial compressive loading and demonstrates the negative Poisson's ratio effect or auxetic behaviour, which is opposite to the usual mechanical deformation behaviour of a material [8–11]. Such auxetic behaviours are observed in natural foams [12–14], cubic elemental metals [15], synthetic kagome lattice structures [11], interlocked cellular structures [16], chiral honeycombs [17] and Bucklicrystals [8], which exhibit attractive mechanical properties such as shear resistance, impact resistance [18] and extraordinary capability

of energy dissipation [10,19,20]. The rational topology optimization of auxetic structures enables the design of 3D architectures with tunable negative Poisson's ratio and mechanical stiffness [8,21,22].

So far, few designs of 3D synthetic auxetic materials have been successfully introduced to the fabrication of products capable of maintaining their auxetic behaviour at large strains. The currently available materials and manufacturing processes are limited to the construction of complex 3D auxetic lattices such as Bucklicrystals with proper mechanical strength and flexibility. As the 3D auxetic lattices usually consist of networks of beams, multipods, and rigid units, the conventional manufacturing methods are time-consuming and expensive to fabricate such complex designs [9]. A few AM techniques such as selective laser melting [16], fused modelling deposition [23] and inkjet printing [9, 17] are able to print two-dimensional (2D) tilting square, triangle, and hexagon or 3D auxetic cellular/chiral lattices, which however cannot satisfy the stringent requirements to sustain large strains and maintain highly recoverable performance [9,21].

Selective laser sintering (SLS) is one of powder-based AM techniques, through which the plastic powders are sintered layer-by-layer to fabricate 3D objects [24–28]. Thermoplastics are mostly used as building materials for the laser sintering process. Thermoplastic elastomers are usually soft and flexible and behave as vulcanized rubbers. Especially, thermoplastic polyurethane (TPU) as a soft shape-memory polymer exhibits the unique thermomechanical storage and strong
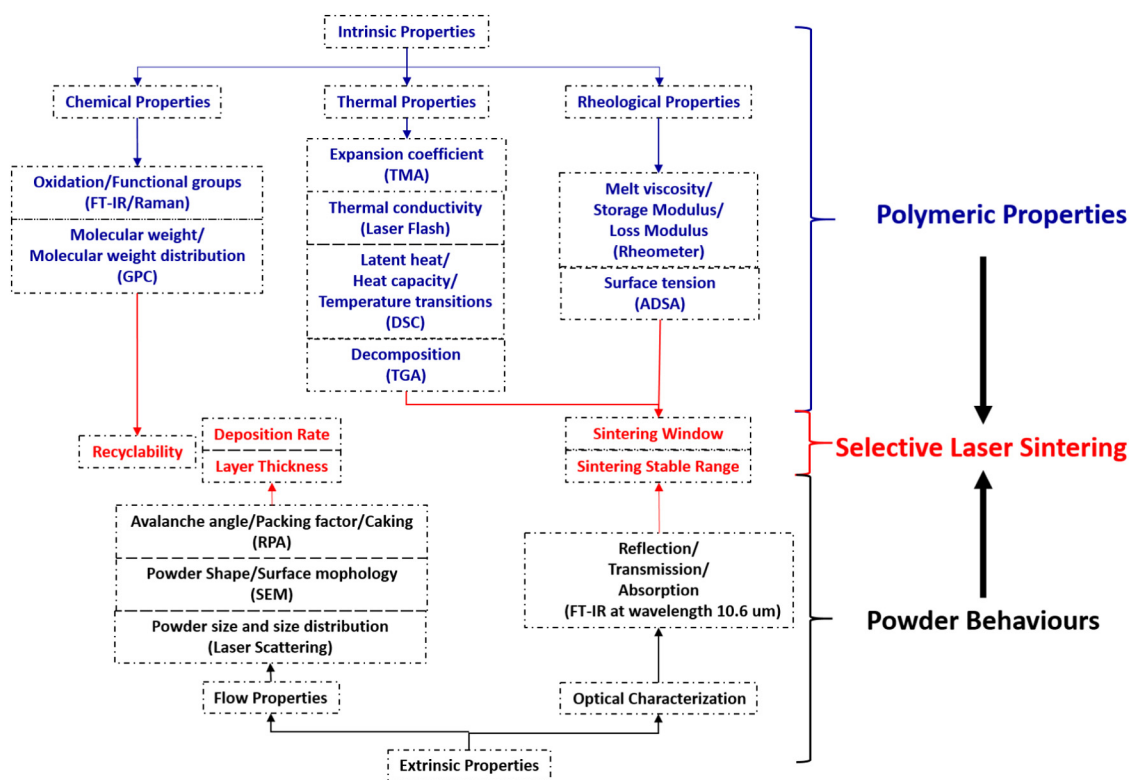
Fig. 1. Illustration of a systematic method for new powder evaluation in the SLS system.

capability of shape recovery upon the cycle of heating-deformation-fixing-recovery. Such properties are enabling the creation of functional active components and extending their service time in end-use applications [29]. Thus, TPU draws the great interest in the fabrications of soft actuators, smart wearable devices, energy storage, vibration resistance and minimally invasive biomedical devices [30,31].

Duel-segment TPU powders consisting of soft and hard phases were introduced to the SLS system in 2013 by BASF Germany company; their sintering behaviours and optimal process parameters have been poorly understood [32]. Meanwhile, the intrinsic thermal behaviours of TPU esters have not been specifically evaluated and validated for the laser sintering system. The soft segments are usually amorphous phase with the glass transition below room temperature; the hard-segment can be a semi-crystalline phase with a relatively high glass transition. The amorphous polymers are not favourable for the laser sintering process because they gradually melt in the wide temperature ranges of melting and slowly solidify as compared with other semi-crystalline polymers. Therefore, how to identify the process temperature and control the preheating still needs investigation. The empirical optimization of processing parameters is based on an iteration of trial and error builds, which is highly time-consuming and extremely expensive depending on the cost per unit of materials.

The specific characteristics of polymer powders, such as their shape, size, flowability and intrinsic thermal behaviours, are combined factors that affect the qualifications and functions of the SLS system. It remains challenge to print objects of complex 3D geometries using TPU powders by laser sintering due to their undesirable shape or size and non-critical melting transition. In the development of new materials for the SLS system, it is critical to validate their feasibility and develop a suitable set of parameters for their powders. Therefore, it is necessary to develop a cost-effective method to evaluate the new type of powders and simplify the optimization process.

In this work, a systematic evaluation of TPU powders was conducted through their flowability and size distribution measurement, thermal transition identification and melting and decomposition energy analysis. The laser sintering processes were optimized to enable the fabrication of the 3D soft auxetic lattices "Bucklicrytals" using the evaluated TPU powders. It shows that the Bucklicrystals retained the buckling-induced negative Poisson's ratio over a wide range of deformation. Cyclic compressive loading was applied to the laser-sintered Bucklicrystals to evaluate their performance of energy dissipation at large strains.

2. Selective laser sintering

2.1. Material evaluation

The process development of SLS is mainly associated with the intrinsic chemical, thermal and rheological properties of the polymers and their physical behaviours in powder form, as illustrated in the schematic flowchart (Fig. 1) where the critical material parameters influencing the SLS process and the relevant characterization methods are highlighted.

In order to determine the SLS process parameters, systematic material evaluation should be conducted to characterize the intrinsic properties of a polymer and the extrinsic properties of its powders which are typically induced by the powder manufacturing process.

The intrinsic properties of the polymer including chemical, thermal and rheological properties are determined by its molecular structure and composition. Rheological testing can be employed to measure the melt viscosity and modulus as these melt behaviours can influence the statue of coalescence powders. The differential scanning calorimetry (DSC) and thermogravimetric analysis (TGA) are applied to identify the phase transition points of polymers. The melt surface tension of polymer can be measured using the axisymmetric drop shape analysis (ADSA). The Fourier transform infrared (FT-IR) or Raman spectroscopy
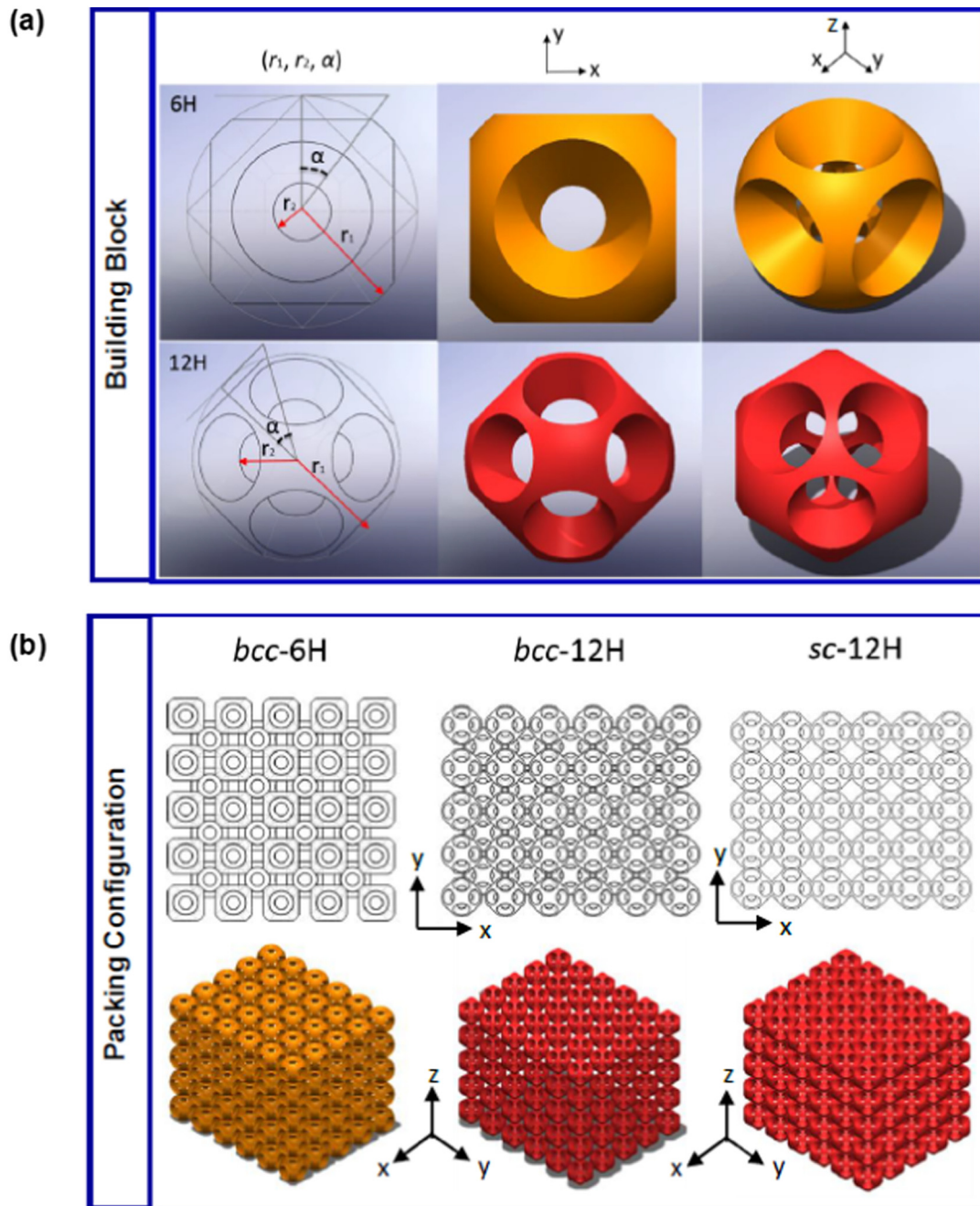
Fig. 2. 3D auxetic lattice via Bucklicrystal were designed through assembling the 6-hole and 12-hole units in the cubic crystal systems of the body center cubic (bcc) and the solid center (sc). The parameters r_1, r_2, and α were monitored to change the porosity and shell thickness of each unit. The three samples of bcc-6H, bcc-12H and sc-12H possess the porosity of 60%.

is used to analysis the chemical composition of polymers or their composites. Molecular weight and its distribution influencing recyclability of materials can be characterized by gel permeation chromatography (GPC).

The two types of extrinsic properties via optical and flow properties of powders are significant to determine the process parameters of the SLS system. The flowability of powders is attributed to their morphology and size distribution, which were characterized by scanning electron microscopy (SEM) and light scatter. The avalanche angle and packing factor measured by Revolution Powder Analyser (RPA) directly reflect the flow properties of powders. The light absorption and scattering at the specific wavelength of laser is utilized to predict the heat absorption of powders induced by laser energy. Therefore, the effective method of process optimization for a new material consists of three steps: (i) powder characterization, (ii) powder feature analysis, and (iii) process parameter setting. This systematic methodology guided the evaluation of TPU powders and narrowed the effective working range of laser energy required for the new material.

2.2. Theoretical model

EOS P395 system (EOS GmbH Munch, Germany) using CO_2 laser with the wavelength at 10.6 μm was employed to sinter polymer powders. Main parameters of sintering process relevant to laser, removal
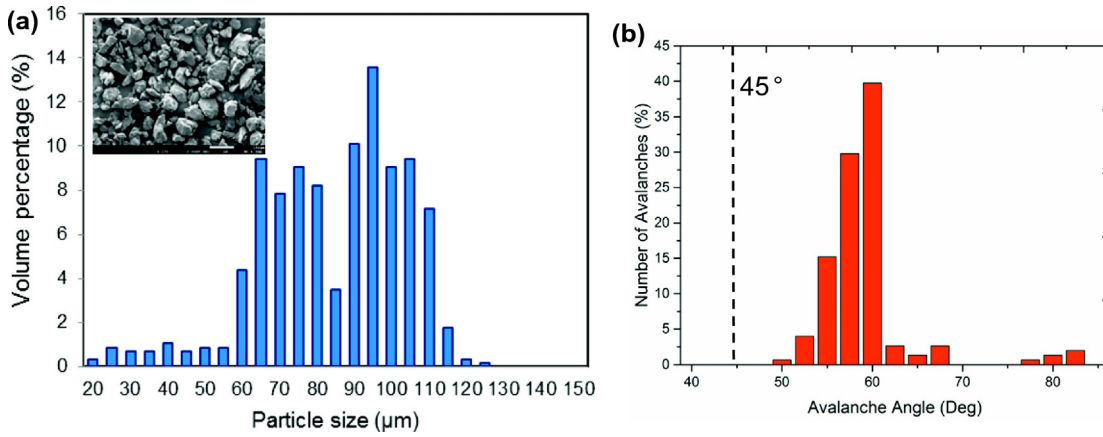
Fig. 3. (a) Size distribution of TPU powders; (b) avalanche angle graph of TPU powders.

chamber and building bed can be monitored in this commercialized system.

Based on the thermal properties of TPU powders, a theoretical method was introduced to narrow down the proper ranges of these parameters and investigate the influences of the sintering parameters. The principles to determine the range of laser input energy were to evaluate the energy required for melting and decomposition for specific polymer powders. Energy per volume required for melting was defined as

$$E_{mv} = \rho^*(T)\phi\int_{T_b}^{T_{mf}} C_p^*(T)dT, (T_b < T < T_{mf}),\qquad(1)$$

and energy absorption per volume within the stable sintering region (SSR) as described.

$$E_{dv} = \rho^*(T)\int_{T_{mf}}^{T_{ds}} C_p^m(T)dT, (T_{mf} < T < T_{ds}),\qquad(2)$$

where T_{ms} and T_{mf} are the onset and offset of melting; T_{ds} is the onset of decomposition where causes the weight loss at 1% of polymer; a ϕ is the packing factor of polymer powders; T_b is the bed temperature of laser sintering. The modified specific heat C_p^* is a function of temperature, it was identified by the modulated DSC measurement. As the amorphous phase is predominated in the TPU polymer, its C_p^* gradually changed within the melting range from the onset to offset temperature. Sintering stable range (SSR) is described the optimum temperature range for successful laser sintering, which usually starts from the offset of melting T_{mf} to the onset of decomposition T_{ds}, which is indicated by the 1% weight loss in the decomposition plot [34].

The critical parameters such as laser power p, scanning speed s, and hatch space h were monitored to control the sintering process because the energy density per volume E_{vol} upon laser scanning is predicted as

$$E_{vol} = \frac{p}{hsL},\qquad(3)$$

where L is the layer thickness of each layer.

To effectively sinter polymer powders and prevent polymer degradation or decomposition, the input laser energy should satisfy a relationship expressed as.

$$E_{mv} < E_{vol}\alpha_c < E_{dv},\qquad(4)$$

where E_{vol} is the laser energy per volume; α_c is the effective heat absorptivity of polymer powders upon laser scanning. This relationship can be employed to predict the proper range of process parameters that induces sufficient energy for melting and remain the heating temperature within the SSR.

3. Material characterizations

Bulky TPU usually has the density of 1.2 g/cm^3, while its powder form (DESMOSINT X92 from BASF Germany) has a mean density of 0.65 g/cm^3. The melting temperature of the TPU powders is around 150 °C, and the melt volume flow rate at 190 °C is 18 cm^3 per 10 min at 190 °C. The surface morphologies of TPU powders and the cross sections of sintered TPU specimens can be observed using a field emission SEM (FESEM) (JSM-7600F, JEOL Ltd., Tokyo, Japan) at 2–5 kV. The light absorptivity of TPU powders at the wavelength of 10.6 μm was
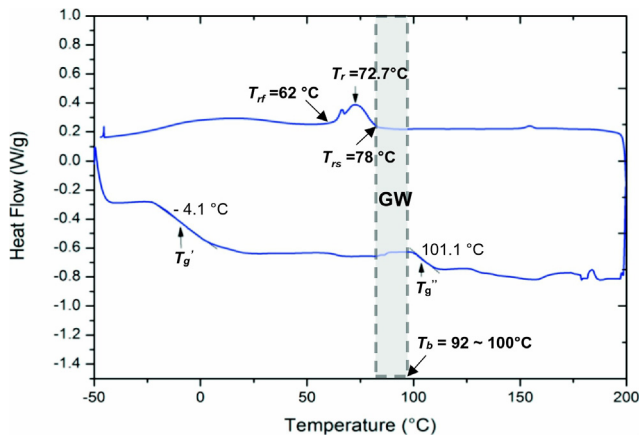

Fig. 4. The endo- and exothermal heat flow of TPU powders was characterized upon heating and cooling from −50 °C to 200 °C at the rate of 10 °C/min. The glass transitions, onset, and offset of recrystallization temperature were indicated. The glass window (GW) for bed temperature control was identified.
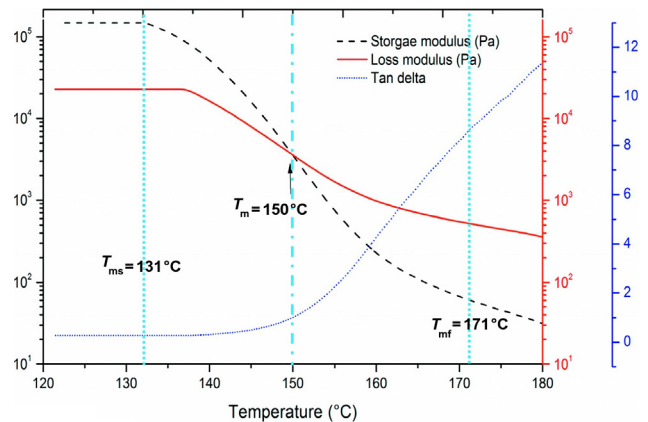

Fig. 5. Rheological testing diagram of TPU powders from – 50 °C to 200 °C at the rate of cooling and heating at 10 °C/min under the angular frequency of 1 rad/s.
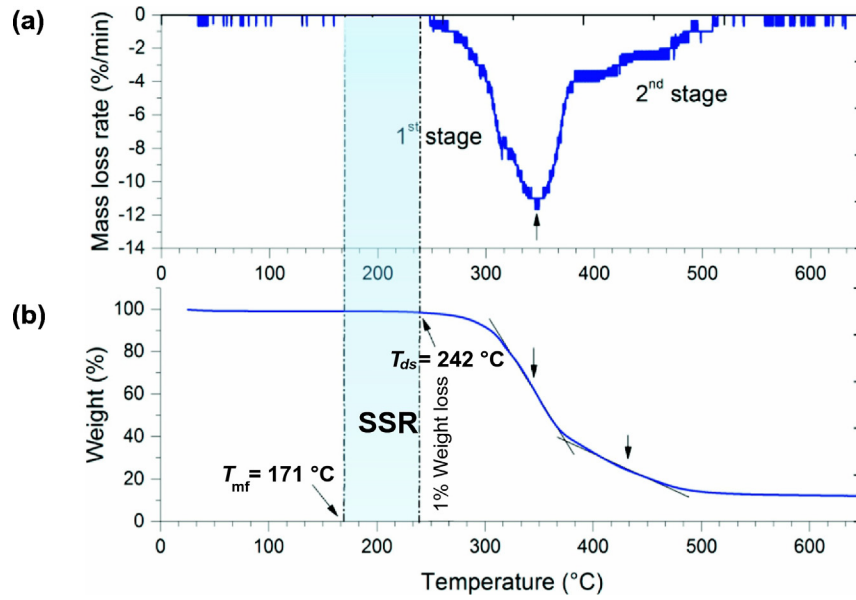
Fig. 6. TGA plots of (a) mass loss rate and (b) weight ratio of TPU decomposition started from 25 °C to 600 °C. The SSR was indicated from the offset of melting to the onset of decomposition.

evaluated by a FT-IR spectroscopy (PerkinElmer Spectrum One FTIR). The avalanche angle of powders to evaluate their flowability were measured by RPA. The instrument was run to obtain the 250 sets of data points corresponding to the information of each powder avalanche.

The glass transitions and the melting range of TPU powders were characterized through the endo- and exothermal processes using DSC Q800 equipment (TA Instruments) under an air atmosphere. The powders of 5 mg were encapsulated in a TA Tzero standard aluminum pan and loaded into DSC. The thermal condition was programmed in the following steps: cooling rapidly to $T = -50$ °C, holding isothermally for 1 min, heating up at the rate of 10 °C/min to 200 °C, holding isothermally for 1 min, cooling down to $T = -50$ °C at the rate of 10 °C/min, and eventually holding isothermally for 1 min to stop.

In addition, a modulated model of DSC was applied to characterize the modified heat capacity of TPU upon its melting process according to the ASTM standard E1269-11 [33]. The modified heat capacities C_p^* from powder phase, melting metaphase and liquid phase were measured, which normally behave as a functional of temperature. This temperature dependent function of $C_p^*(T)$ was utilized to further predict of heat absorption of TPU at different stages of the sintering process.

The decomposition temperatures of TUP materials were identified using TGA Q500 equipment (TA instrument), in which the TPU powders with the mass of 15 mg were heated from the room temperature to 650 °C under N_2 gas environment.

Rheological dynamic measurements were performed in the strain controlled DHR-Rheometer (TA-Instruments), using the 25 mm-diameter parallel plates. The powders were compressed into a cylinder
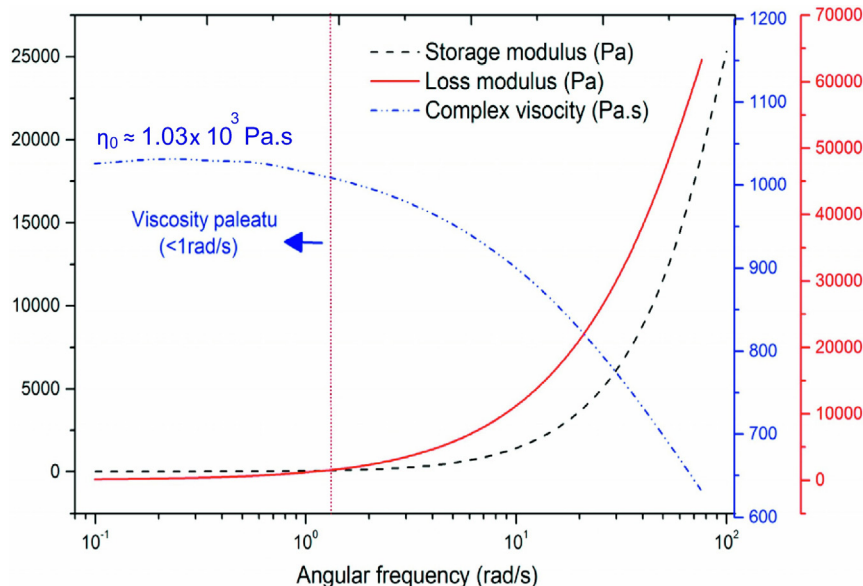

Fig. 7. Storage and loss moduli of the fully melted TPU and its melt viscosity over the range of angular frequency range from 0.1 to 100 rad/s at the temperature of 180 °C.
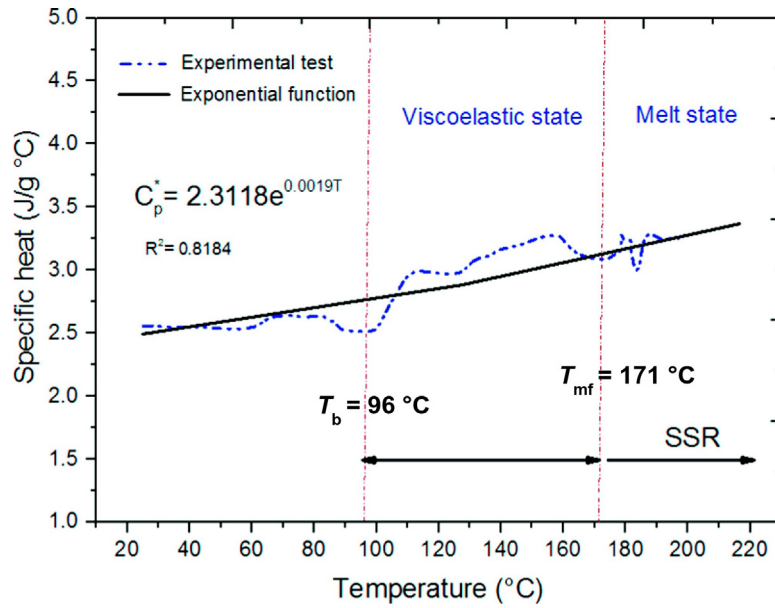
Fig. 8. The plot of the temperature-dependent specific heat of TPU powders from the powder phase to the melting metaphase to the liquid phase.

(25 mm-diameter and 2 mm-thickness) by mechanical force. Firstly, the melt viscoelastic storage modulus, loss modulus and loss factor of TPU were measured within the range from 100 °C to 200 °C. Secondly, the specimens of TUP were tested in a dynamic mode, the frequency was varied from 100 to 0.1 rad/s and the melt viscoelastic storage shear modulus and loss shear modulus were investigated at 180 °C.

4. Design of Bucklicrystals

Babaee et al. designed a new group of 3D metamaterials "Bucklicrystals" and investigated their buckling-induced auxetic behaviour using a non-linear finite element analysis [8]. In these designs, elastomeric spherical shells with 6-hole or 12-hole were arranged periodically to construct 3D body center cubic (bcc) and simple cubic (sc) structures as schematically illustrated in Fig. 2. The two types of soft building blocks can construct three types of packing configurations of bcc-6H, bcc-12H, and sc-12H.

Under compressive loading, the 3D periodic, soft and porous structures are buckled and the connecting nodes are rotating, leading to the volume shrinkage along two transverse directions. In order to ensure the large volume shrinkage of the entire lattice, Bucklicrystals are required to compose of soft and highly ductile materials, as the localized regions e.g. the connected nodes and beams experience the extremely large local strains.

The dimensions of building blocks including inner diameter r_1, outer diameter r_2, and projection angle α, can decide the porosity and shell thickness of each unit and the configurations of assembled structures in the cubic crystal systems. Whereas, a trade-off exists between optimal strength of structure and maximum of strain deformation, when the dimensional factors are being modulated. In this work, the parameters of r_1, r_2, and α in 6-hole and 12-hole units were monitored to achieve the identical porosity of 60% and the size and dimensional accuracy of printed lattices were mainly limited by the laser sintering process.

5. Results and discussion

5.1. Evaluation of TPU powders

In the pre-sintering steps, powder evaluation usually includes the measurements of size distribution, flowability, endo- and exothermal and rheological properties of polymer powders. The size range determines the minimum layer thickness upon deposition; the proper flowability of powders enables to ensure the uniform deposition of each layer. It is observed that the irregular TPU powders were with a relatively wide size distribution from 60 to 110 μm (Fig. 3(a)). As a result, the avalanche angle of TPU powders was much higher than 45°, below which usually the powders flow properly to be deposited during the printing process. Such inferior flow behaviour is not preferable in the SLS process because it may adversely affect the layer-by-layer deposition. Unfortunately, these irregular TPU powders could still be deposed uniformly in the EOS P395 system, even their flowability is not comparable with that of semi-spherical polymer powders [27].

Compared with semi-crystalline polymers such as polyethylene and polyamides (PA 12 and PA 11), the duel-segment TPU are mainly consisting of the amorphous phase with no critical melting point.

Table 1
Material properties of TPU powders.

Material properties	Value
Specific heat C_p^*, (J/g °C)	$2.31e^{0.0019T}$
Melting temperature T_m, (°C)	150
Recrystallization peak T_r, (°C)	78
Enthalpy of recrystallization ΔH_r, (J/g)	46.11
Modified density ρ^*, (g/cm³)	1.2
Packing fraction ϕ,	0.48
Onset melting temperature T_{ms}, (°C)	131
Offset melting temperature T_{mf}, (°C)	171
Onset recrystallization temperature T_{rs}, (°C)	78
Offset recrystallization temperature T_{rf}, (°C)	62
Glass window width (GW), (°C)	17.99
Stable sintering region (SSR), (°C)	171–242
Melt viscosity η at 0.1 rad/s, (Pa·s)	1.03×10^3
Light absorptivity α at 10.6 μm, (%)	18

Note: T is instant temperature of polymer powders or melts during sintering process.

Table 2
Evaluations of E_{mm}, E_{mv}, E_{dm} and E_{dv} for TPU powders and prediction for the effective range of E_{vol} corresponding to SSR of TPU.

Energy parameter	Value
Mass energy for melting E_{mm} (J/g)	119.5
Volume energy for melting E_{mv} (J/mm³)	0.068
Mass energy before decomposition E_{dm} (J/g)	192.3
Volume energy before decomposition E_{dv} (J/mm³)	0.231
Energy input range of laser E_{vol} (J/mm³)	0.378–1.283

Table 3
Laser sintering parameters in the EOS P395 system.

Process parameter	Value
Laser power p (W)	8, 10, 12, 14
Scanning speed s (mm/s)	3000, 4000
Hatching spacing h (mm)	0.1
Bed temperature T_b (°C)	96
Chamber temperature T_c (°C)	60
Layer thickness h (μm)	100

Additionally, the thermal behaviours of TPU powders were addressed to determine the process parameters, as these critical transitions during the cycle of heat absorption and release are the essential indicators to predict the parameter ranges of laser sintering [27,35,36]. DSC is a standard approach to determine the glass transition temperature (T_g), the melting point (T_m) and the recrystallization temperature (T_r), which are significant to predict the working temperature ranges of powder bed and removal chamber. Usually, polyurethanes are composed of the soft and stiff segments, the T_g of TPU can be tailored by controlling the composition of each segment. TPU elastomers can be flexible at the room temperature because the soft and amorphous phases are predominated in the matrix. As illustrated in Fig. 4, TPU powders exhibited two glass transitions of T_g' and T_g'', the soft segments were with a low T_g' at −4 °C and have no critical melting point; the hard segments showed a high T_g'' at 101 °C. However, the melting of TPU powders occurred in the range of temperature from 120 °C to 180 °C. Meanwhile, the recrystallization peak located at 72.74 °C and the entire recrystallization ranged from 78 °C to 62 °C. These observations indicate that the soft segments are amorphous structures and the hard segments are semicrystalline structures. The semi-crystallized hard segments experience dramatic the phase change and volume shrinkage during recrystallization [37]. Thus, the removal chamber temperature needs to be set just below the offset of recrystallization to secure a stable arrangement of polymer segments after solidification and minimize the dimensional shrinkage of printed parts.

The glass window (GW) was defined as the temperature difference between the onset of recrystallization and onset of melting. This temperature range can be used to evaluate the processibility of polymers in the SLS system. However, the melting temperature of TPU is not obvious, the rheological testing was employed to investigate the melting behaviours of TPU powders through measuring the storage and loss modulus over the melting range.

In the rheological study, polymer behaves as solid manner within the temperature range, where the storage modulus is higher than loss modulus. In contrast, the loss modulus is higher than the storage modulus at the liquid state. In addition, the storage modulus drops dramatically until it fully melted. As illustrated in Fig. 5, the melting point of TPU presented at 150 °C. The storage modulus dropped from 131 °C and approached to flat at 171 °C, correspondingly, the onset and offset of melting were located at 131 °C and 171 °C, respectively.

Fig. 6 shows that the decomposition of TPU started from 242 °C and two stages of decomposition were observed due to the presence of dual-segments in the polymer matrix. The SSR via range between the offset of melting and the onset of decomposition was identified in Fig. 6(b), it ranged from 171 °C to 242 °C which is relatively narrow as compared with PA12 from 198 °C to 360 °C [27]. As a result, the energy input from laser needs to be precisely controlled to maintain the sintering temperature within the SSR.

Fig. 7 shows that the melt viscosity of TPU exhibited a plateau at the low-frequency range (<1 rad/s) but dropped dramatically when the angular frequency increased above 1 rad/s at an isothermal condition around 180 °C. The zero-shear melt viscosity strongly impacted on the state of coalescence as revealed by the Frenkel's relation. The viscous sintering of polymer powders was described by the simplified Frenkel's model [25,26,38]

$$\frac{x^2}{R} = \frac{2\Gamma}{3\eta_0}t,$$

(5)

where x and R are necking and particle radius, respectively; Γ is surface tension and η_0 is zero-shear viscosity of the polymer melt; t is sintering time. This function reveals that the melt viscosity is a critical factor to judge the sinterability of powders as compared with the surface tension, which is weakly affected by temperature change. It also indicates that the increase of fusion time enable to overcome the insufficient coalescence caused by the undesirable morphology of powders and relatively high zero-shear viscosity [38,39]. At the low angular frequency range (<1 rad/s), TPU is with the melt viscosity of 1.03×10^3 Pa at the low frequency range, which is close to that value of PA12 (1.4×10^3 Pa·s) [27], and thus the melt viscosity of TPU should not limit the fully fusion of powders thermodynamically.

Additionally, the modulated specific heat C_p^* of TPU over the temperature range from powder phase to melting metaphase to liquid phase were plotted in Fig. 8. The exponential function was applied to describe the trend of C_p^* over the process temperature range. It was further utilized to evaluate energy absorptions at the stages of melting and decomposition.
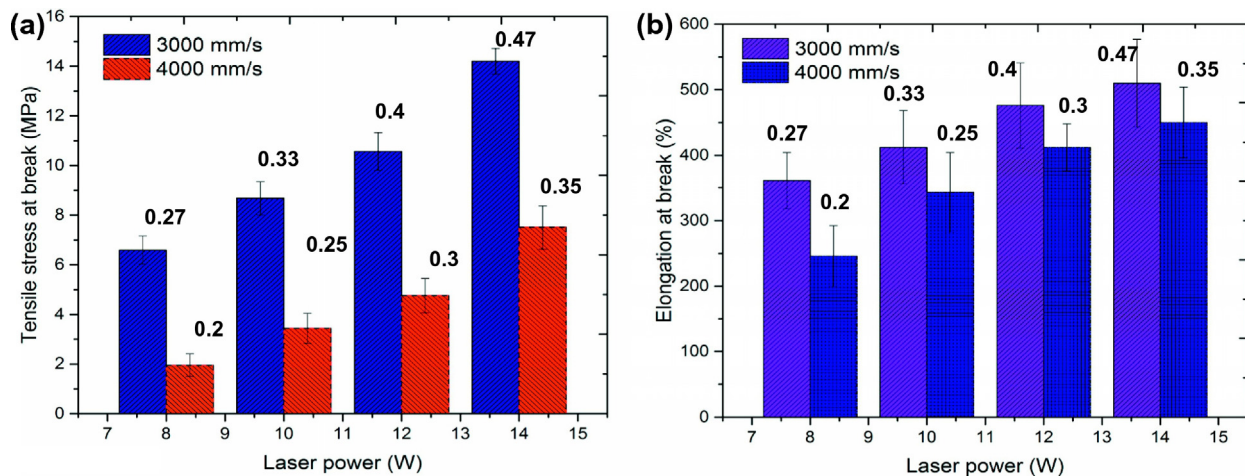

Fig. 9. Evaluations of the SLS specimens fabricated upon different sets of parameters (a) the tensile stress at break and (b) the elongation at break. The volumetric energy densities of different combinations of parameters are indicated with the unit J/mm^3.
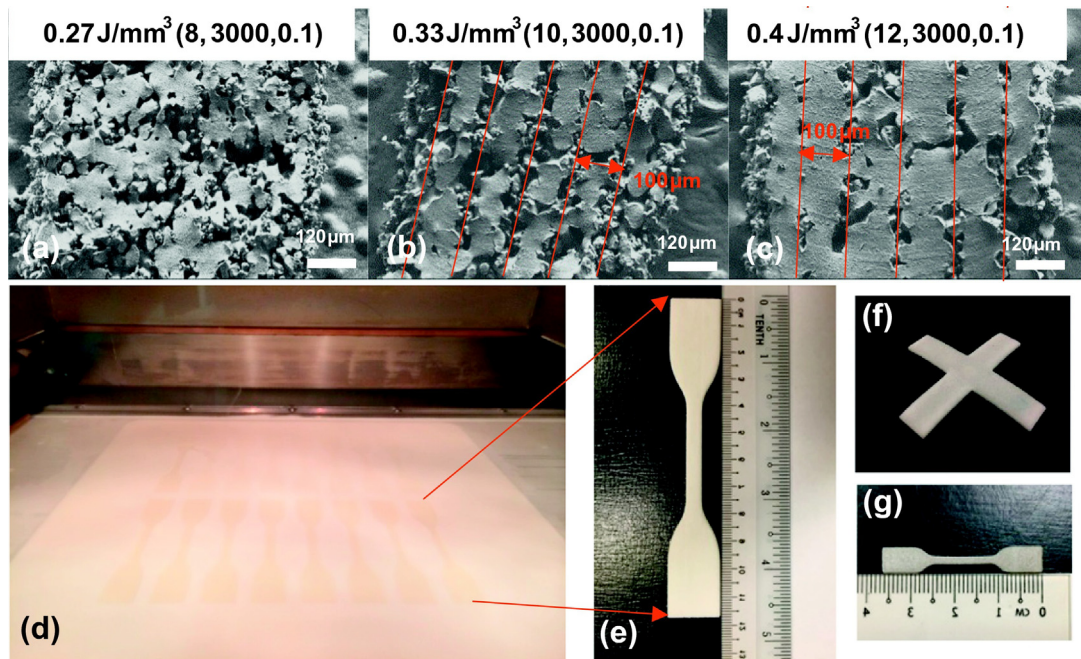
Fig. 10. The cross-section of sintered specimens of TPU produced at varied powers (a) 8 W, (b) 10 W and (c) 12 W with the bed temperature (96 °C), scanning speed (3000 mm/s) and hatching space (0.1 mm); (d) the building bed of laser sintering within the heating chamber; (e) the dogbone tensile bar (ASTM D638 Type IV) for tensile testing; (f) and (g) the printed samples for warping and elongation testing, respectively.

5.2. Process optimization

According to the list of material properties in Table 1, the cooling chamber temperature was set at 60 °C as suggested just below the re-crystallization range. The powder bed temperature was 92 °C to 100 °C just below the T_g'' as observed in a powder deposition process. This is because the polymer powders were tending to agglomerate with a caking effect once the bed temperature increased above 103 °C. The evaluations of energy required for melting and decomposition have been conducted and the values of energy required were listed in Table 2.

If TPU powders were with an effective light absorptivity of 18%, the range of E_{vol} was predicted from 0.378 to 1.283 J/mm^3 through the relationship described in Eq. (4). Within the narrowed E_{vol} range, two factors of laser power and scanning speed were tailored to investigate the influences of laser parameters, which were separately set in the distinct levels (Table 3).

The tensile properties such as tensile stress and elongation at break of laser-sintered specimens are shown in Fig. 9, corresponding to the different combinations of process parameters. The energy densities of

Table 4
The optimized process parameters for TPU to produce complex geometric objects.

Process parameter		
Laser power p, (W)	Hatching	12
	Contour 1, Contour 2	14, 14
	Edge 1, Edge 2	14, 14
Scanning speed s, (mm/s)	Hatching	2000
	Contour 1, Contour 2	3000
	Edge 1, Edge 2	3000
Hatching spacing h, (mm)		0.1
Bed temperature T_b, (°C)		96
Chamber temperature T_c, (°C)		60
Layer thickness L, (μm)		100

each set of parameters were labelled on the diagrams. According to the predicted effective range of E_{vol}, the input laser energy was sufficient to fully melt the powers above the level of 0.4 J/mm^3. The obtained elongation strain approaching to 500% has qualified the use of constructing the 3D soft metamaterials to sustain large strains.

Usually, the tensile strength and elongation at break both decrease, as the scanning speed increases or the laser power drops. The scanning speed determines the duration of exposure time for powders to be sintered; the laser power indicates the inputted thermal energy onto the powder bed in unit time. The tensile strength considerably decreases when the scanning speed increases from 3000 mm/s to 4000 mm/s, thus the lower scanning speed is preferable to control the coalescence among powders. The SLS process only undergoes the internal driving force of melting flow without the external force for the coalescence.

In Fig. 10(a–c), the SEM images show that the gasses trapped among the interspace of powders were difficult to be removed. Therefore, the cross-sections of sintered parts show that the powders could not fuse fully in the inter-plane (X-Y plane) and out-plane (Z axis) direction when input laser energy was below 4 J/mm^3. However, in the out-plane direction, the interlayer voids were still presenting even the laser power increasing to 0.4 J/mm^3. This is mainly due to the poor heat penetration of laser, as TPU powders are closely packed and weakly thermal conductive. If the exposure time to the laser is extremely short, the instant coalescence among powders is limited by the fusion kinetics as explained in Frenkel's theory of sintering [27,38]. Therefore, the scanning speed can be even reduced from 3000 mm/s and correspondingly the laser power need to increase slightly to secure sufficient thermal energy for melting.

On the other hand, it was observed that the powders started to decompose with smoky dust once the laser powder increase above 15 W, even the input laser energy per volume was still lower than the up limit 1.283 J/mm^3. As the laser heat distribution follows Gaussian profile, the localized temperature upon powder bed is higher than the onset of decomposition 242 °C. Therefore, to reduce the scanning
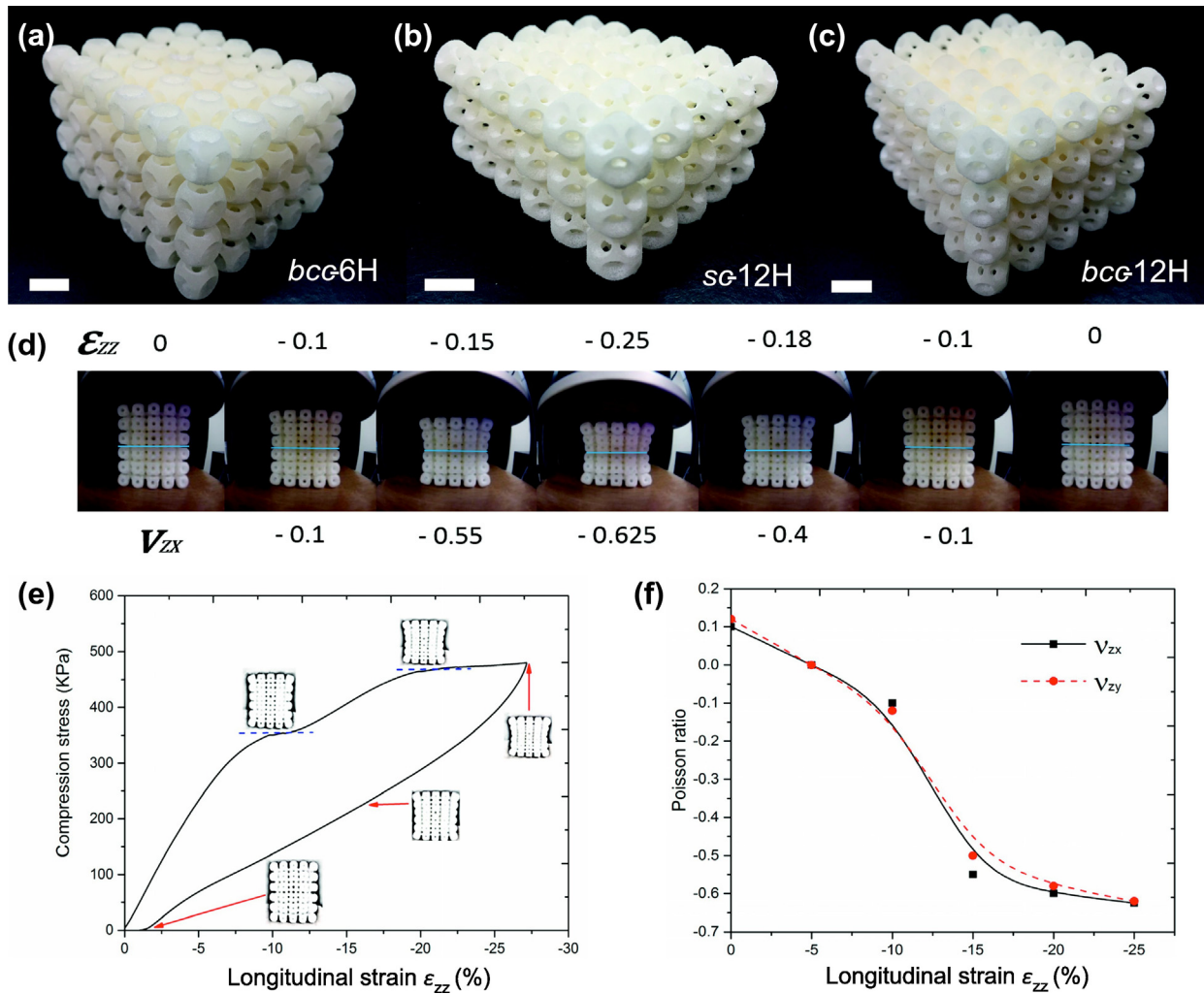
Fig. 11. 3D complex auxetic lattices (a) *bcc*-6 hole, (b) *sc*-12 hole and (c) *bcc*-12 hole (The scale bars are 1 cm); (d) the photos of the progressive deformation of *bcc*-6 hole structures; (e) the compression-relaxation stress-strain curve and (f) both Poisson's ratios ν_{xz} and ν_{yz} vs. longitudinal strain ε_{zz} of *bcc*-6 hole Bucklicrystal made of laser-sintered TPU.

speed is effective to improve the fusion of powders and print soft and flexible metamaterials.

The optimal parameter set was applied to print 3D complex geometric as listed in Table 4. This set can minimize the degradation of

polymers under heating and maintain the acceptable mechanical strength and outstanding ductility and flexibility of TPU. The double contour and edge were applied to improve the dimensional accuracy and surface features.
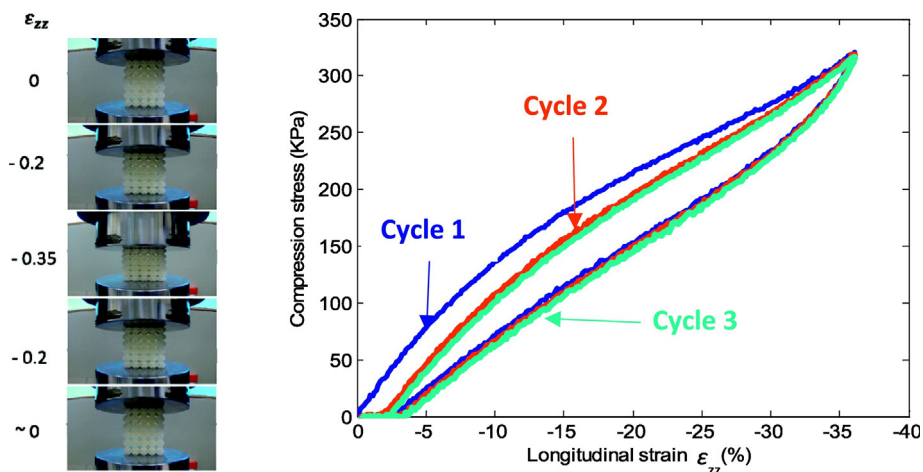

Fig. 12. The 3 cycles of stress-strain curve for the lattice structure *sc*-12H upon the loading and unloading at a strain rate of 1 mm/s.

5.3. Fabrication of 3D soft auxetic lattice structures

The laser-sintered TPU auxetic structures are shown in Fig. 11(a–c) corresponding to the designs of *bcc*-6H, *sc*-12H and *bcc*-12H. The basic units were printed in 3D to form Bucklicrystals with a negative Poisson's ratio, and the 6-hole *bcc* Bucklicrystal was uniaxially compressed to investigate its buckled configurations as shown in Fig. 11(d). The deformation of *bcc*-6H array was captured by taking photographic every 5 s at the applied normal strain with the rate of 1 mm/s, also the recovery of structure was also investigated upon release of the applied vertical displacement. The lateral boundaries of the laser-sintered TPU structure bent inwards, a clear indication of a 3D negative Poisson's ratio. Both transverse strains ε_{xx} and ε_{yy} decreased indicating that the structure contracts in both lateral boundaries. The Poisson's ratios were calculated from the engineering strains as $\nu_{ij} = -\varepsilon_{ii}/\varepsilon_{jj}$. The evolution of ν_{xz} and ν_{yz} were plotted as functions of ε_{zz} shown in Fig. 11(f). Initially, both Poisson ratios decreased gradually till $\varepsilon_{zz} = -0.05$, and then dramatically dropped to the value of $\nu \approx -0.6$ and plateau at $\varepsilon_{zz} = -0.2$. This demonstrated that the laser-sintered Bucklicrystal can maintain the auxetic behaviour over the wide range of deformation. The corresponding compressive stress-strain curve (Fig. 11(e)) was also indicated that the structural transformations induced by instabilities occurred when the Bucklicrystal was compressed at the different levels of strains.

Such 3D soft auxetic lattices possess high potential applications in damping, energy absorption, and mechanical actuation. The cyclic loading-unloading of the *sc*-12H structure was conducted to investigate its compressive behaviour and recoverability. The lattice structure underwent a softening effect over the first cycle and became slightly complaint from the second cycle onwards. The recovery curves followed the same path regardless of loading cycles. The residual strain of entire *sc*-12H structure maintained at 2– 3%, which is much lower than the instantly recoverable strain of 10– 20% for the laser-printed neat PU in the dog-bone shape [35]. Therefore, the stress-strain loops exhibited highly recoverable and repeatable behaviours, as the TPU retained the elastomeric properties even after constructed the complex 3D geometries by laser sintering. The energy dissipation of each cycle can be predicted through a hyperelastic model with Mullins effect as investigated by Shen et al. [40], which considered the soften effect at first loop and well predicted the cycling compression-relaxation behaviours in energy aspects. Therefore, the proper model integrated the non-linear behaviours of material and structure can effectively guide a new generation of 3D design for additive manufacturing, and the systematic selection and evaluation process of materials are beneficial for the process development and optimization of the manufacturing technique (Fig. 12).

6. Conclusion

This work presents a systematic investigation on the fabrication of 3D soft auxetic lattice structures via SLS, including the rational choice of TPU powders, evaluation of physical and thermal properties of powders, optimization of the manufacturing process and mechanical testing of 3D-printed structures. The laser-sintered Bucklicrystals could sustain a wide range of compressive strains and the transverse directions of lattice structures shrunken under compressive loading. The soft TPU auxetic lattices were capable of withstanding repeated compression cycles over large deformations. The work explored the large potential of 3D-printed auxetic lattices for energy absorption and mechanical damping applications. Importantly, the concept of Manufacturing for Design was well implemented and demonstrated through using TPU to fabricate 3D auxetic lattice by laser sintering, integrating of suitable material and technology to serve the desirable structural products.

References

[1] C.K. Chua, K.F. Leong, 3D Printing and Additive Manufacturing: Principles and Applications, World Scientific Publishing Company Pte Limited, 2014.
[2] C.K. Chua, K.F. Leong, K.H. Tan, F.E. Wiria, C.M. Cheah, Development of tissue scaffolds using selective laser sintering of polyvinyl alcohol/hydroxyapatite biocomposite for craniofacial and joint defects, J. Mater. Sci. Mater. Med. 15 (10) (2004) 1113–1121.
[3] Z.X. Khoo, J.E.M. Teoh, Y. Liu, C.K. Chua, S. Yang, J. An, K.F. Leong, W.Y. Yeong, 3D printing of smart materials: a review on recent progresses in 4D printing, Virt. Phys. Prot. 10 (3) (2015) 103–122.
[4] B.S. Bucklen, W.A. Wettergreen, E. Yuksel, M.A.K. Liebschner, Bone-derived CAD library for assembly of scaffolds in computer-aided tissue engineering, Virt. Phys. Prot. 3 (1) (2008) 13–23.
[5] M. Vaezi, S. Yang, Extrusion-based additive manufacturing of PEEK for biomedical applications, Virt. Phys. Prot. 10 (3) (2015) 123–135.
[6] W.S. Tan, C.K. Chua, T.H. Chong, A.G. Fane, A. Jia, 3D printing by selective laser sintering of polypropylene feed channel spacers for spiral wound membrane modules for the water industry, Virt. Phys. Prot. 11 (3) (2016) 151–158.
[7] V. Francis, P.K. Jain, Experimental investigations on fused deposition modelling of polymer-layered silicate nanocomposite, Virt. Phys. Prot. 11 (2) (2016) 109–121.
[8] S. Babaee, J. Shim, J.C. Weaver, E.R. Chen, N. Patel, K. Bertoldi, 3D soft metamaterials with negative Poisson's ratio, Adv. Mater. 25 (36) (2013) 5044–5049.
[9] K. Wang, Y.-H. Chang, Y. Chen, C. Zhang, B. Wang, Designable dual-material auxetic metamaterials using three-dimensional printing, Mater. Des. 67 (2015) 159–164.
[10] J. Shim, S. Shan, A. Kosmrlj, S.H. Kang, E.R. Chen, J.C. Weaver, K. Bertoldi, Harnessing instabilities for design of soft reconfigurable auxetic/chiral materials, Soft Matter 9 (34) (2013) 8198–8202.
[11] G. Wu, Y. Cho, I.-S. Choi, D. Ge, J. Li, H.N. Han, T. Lubensky, S. Yang, Directing the deformation paths of soft metamaterials with prescribed asymmetric units, Adv. Mater. 27 (17) (2015) 2747–2752.
[12] J.P. Kruth, P. Mercelis, J. Van Vaerenbergh, L. Froyen, M. Rombouts, Binding mechanisms in selective laser sintering and selective laser melting, Rapid Prototyp. J. 11 (1) (2005) 10.
[13] R. LAKES, Foam structures with a negative Poisson's ratio, Science 235 (4792) (1987) 1038–1040.
[14] R. Zach, S.L. Roderic, Cosserat elasticity of negative Poisson's ratio foam: experiment, Smart Mater. Struct. 25 (5) (2016) 054004.
[15] R.H. Baughman, J.M. Shacklette, A.A. Zakhidov, S. Stafstrom, Negative Poisson's ratios as a common feature of cubic metals, Nature 392 (6674) (1998) 362–365.
[16] X. Wang, X. Li, L. Ma, Interlocking assembled 3D auxetic cellular structures, Mater. Des. 99 (2016) 467–476.
[17] D. Mousanezhad, S. Babaee, H. Ebrahimi, R. Ghosh, A.S. Hamouda, K. Bertoldi, A. Vaziri, Hierarchical honeycomb auxetic metamaterials, Sci. Rep. 5 (2015) 18306.
[18] D. Olly, F. Leon, S. Terry, A. Andrew, A. Tom, Quasi-static characterisation and impact testing of auxetic foam for sports safety applications, Smart Mater. Struct. 25 (5) (2016) 054014.
[19] A. Lazarus, P.M. Reis, Soft actuation of structured cylinders through auxetic behavior, Adv. Eng. Mater. 17 (6) (2015) 815–820.
[20] Z.G. Nicolaou, A.E. Motter, Mechanical metamaterials with negative compressibility transitions, Nat. Mater. 11 (7) (2012) 608–613.
[21] A. Clausen, F. Wang, J.S. Jensen, O. Sigmund, J.A. Lewis, Topology optimized architectures with programmable Poisson's ratio over large deformations, Adv. Mater. 27 (37) (2015) 5523–5527.
[22] R. Xin, S. Jianhu, G. Arash, T. Hongqi, X.Y. Min, A simple auxetic tubular structure with tuneable mechanical properties, Smart Mater. Struct. 25 (6) (2016) 065012.
[23] C.S. Ha, M.E. Plesha, R.S. Lakes, Chiral three-dimensional isotropic lattices with negative Poisson's ratio, Phys. Status Solidi B 253 (7) (2016) 1243–1251.
[24] J. Bai, S. Yuan, W. Chow, C.K. Chua, K. Zhou, J. Wei, Effect of surface orientation on the tribological properties of laser sintered polyamide 12, Polym. Test. 48 (2015) 111–114.
[25] J.M. Bai, R.D. Goodridge, R.J.M. Hague, M. Song, Improving the mechanical properties of laser-sintered polyamide 12 through incorporation of carbon nanotubes, Polym. Eng. Sci. 53 (9) (2013) 1937–1946.
[26] J. Bai, R.D. Goodridge, R.J.M. Hague, M. Song, M. Okamoto, Influence of carbon nanotubes on the rheology and dynamic mechanical properties of polyamide-12 for laser sintering, Polym. Test. 36 (0) (2014) 95–100.
[27] S. Yuan, J. Bai, C. Chua, J. Wei, K. Zhou, Material evaluation and process optimization of CNT-coated polymer powders for selective laser sintering, Polymers 8 (10) (2016) 370.
[28] S.F. Wen, C.Z. Yan, Q.S. Wei, L.C. Zhang, X. Zhao, W. Zhu, Y.S. Shi, Investigation and development of large-scale equipment and high performance materials for powder bed laser fusion additive manufacturing, Virt. Phys. Prot. 9 (4) (2014) 213–223.
[29] J. Raasch, M. Ivey, D. Aldrich, D.S. Nobes, C. Ayranci, Characterization of polyurethane shape memory polymer processed by material extrusion additive manufacturing, Addit. Manuf. 8 (2015) 132–141.

[30] J. Robertson, A. Torbati, E.D. Rodriguez, Y. Mao, R.M. Baker, H.J. Qi, P.T. Mather, Mechanically programmed shape change in laminated elastomeric composites, Soft Matter 11 (28) (2015) 5754–5764.

[31] B. Matteo, S. Fabrizio, Vibration transmissibility and damping behaviour for auxetic and conventional foams under linear and nonlinear regimes, Smart Mater. Struct. 22 (8) (2013) 084010.

[32] K. Plummer, M. Vasquez, C. Majewski, N. Hopkinson, Study into the recyclability of a thermoplastic polyurethane powder for use in laser sintering, P I Mech Eng B-J Eng. (2012).

[33] R.L. Danley, New heat flux DSC measurement technique, Thermochim. Acta 395 (1–2) (2003) 201–208.

[34] M. Vasquez, B. Haworth, N. Hopkinson, Methods for quantifying the stable sintering region in laser sintered polyamide-12, Polym. Eng. Sci. 53 (6) (2013) 1230–1240.

[35] S. Yuan, J. Bai, C.K. Chua, K. Zhou, W. Jun, Characterization of creeping and shape memory effect in laser sintered thermoplastic polyurethane, J. Comput. Inf. Sci. Eng. 16 (4) (2016) 041007.

[36] S. Berretta, K.E. Evans, O. Ghita, Predicting processing parameters in High Temperature Laser Sintering (HT-LS) from powder properties, Mater. Des. 105 (2016) 301–314.

[37] R.D. Goodridge, C.J. Tuck, R.J.M. Hague, Laser sintering of polyamides and other polymers, Prog. Mater. Sci. 57 (2) (2012) 229–267.

[38] M.M. Ristić, S. Milosević, Frenkel's theory of sintering, Sci. Sinter. 38 (1) (2006) 7–11.

[39] C.L. Yu, D.P. Gao, C.B. Xu, N.B. Tang, T. Zhao, Interpretation of Frenkel's theory of sintering considering evolution of activated pores: I. Confirmation of the time constant, Sci. Sinter. 46 (2) (2014) 141–147.

[40] F. Shen, S. Yuan, Y. Guo, B. Zhao, J. Bai, M. Qwamizadeh, C.K. Chua, J. Wei, K. Zhou, Energy absorption of thermoplastic polyurethane lattice structures via 3D printing: modeling and prediction, Int. J. Appl. Mech. 08 (07) (2016).